



HAL
open science

The Arabidopsis N-alpha-acetyltransferase NAA60 locates to the plasma membrane and is vital for the high salt stress response

Eric Linster, Dominik Layer, Willy V Bienvenut, Trinh V. Dinh, Felix A. Weyer, Wiebke Leemhuis, Annika Brünje, Marion Hoffrichter, Pavlina Miklankova, Jürgen Kopp, et al.

► To cite this version:

Eric Linster, Dominik Layer, Willy V Bienvenut, Trinh V. Dinh, Felix A. Weyer, et al.. The Arabidopsis N-alpha-acetyltransferase NAA60 locates to the plasma membrane and is vital for the high salt stress response. *New Phytologist*, 2020, 228 (2), pp.554-669. 10.1111/nph.16747 . hal-02989484

HAL Id: hal-02989484

<https://hal.science/hal-02989484>

Submitted on 10 Nov 2020

HAL is a multi-disciplinary open access archive for the deposit and dissemination of scientific research documents, whether they are published or not. The documents may come from teaching and research institutions in France or abroad, or from public or private research centers.

L'archive ouverte pluridisciplinaire **HAL**, est destinée au dépôt et à la diffusion de documents scientifiques de niveau recherche, publiés ou non, émanant des établissements d'enseignement et de recherche français ou étrangers, des laboratoires publics ou privés.



Distributed under a Creative Commons Attribution - NonCommercial - NoDerivatives 4.0 International License

The Arabidopsis N^α-acetyltransferase NAA60 locates to the plasma membrane and is vital for the high salt stress response

Eric Linster^{1*} , Dominik Layer^{2*} , Willy V. Bienvenu³ , Trinh V. Dinh¹, Felix A. Weyer², Wiebke Leemhuis¹ , Annika Brünje⁴ , Marion Hoffrichter¹, Pavlina Miklankova¹ , Jürgen Kopp² , Karine Lapouge² , Julia Sindlinger⁵ , Dirk Schwarzer⁵ , Thierry Meinnel³ , Iris Finkemeier⁴ , Carmela Giglione³ , Ruediger Hell¹ , Irmgard Sinning²  and Markus Wirtz¹ 

¹Centre for Organismal Studies Heidelberg, Heidelberg University, Heidelberg 69120, Germany; ²Heidelberg University Biochemistry Center, Heidelberg 69120, Germany; ³Institute for Integrative Biology of the Cell (I2BC), CEA, CNRS, Univ. Paris-Sud, Université Paris Saclay, Gif-sur-Yvette Cedex 91198, France; ⁴Plant Physiology, Institute of Plant Biology and Biotechnology, University of Muenster, Münster 48149, Germany; ⁵Interfaculty Institute of Biochemistry, University of Tübingen, Tübingen 72076, Germany

Summary

Authors for correspondence:

Markus Wirtz

Tel: +49 6221 545334

Email: markus.wirtz@cos.uni-heidelberg.de

Irmgard Sinning

Tel: +49 6221 544781

Email: irmi.sinning@bzh.uni-heidelberg.de

Received: 2 January 2020

Accepted: 13 May 2020

New Phytologist (2020) 228: 554–569

doi: 10.1111/nph.16747

Key words: *Arabidopsis thaliana*, high-salt stress, NAA60, N-terminal acetylation, plasma membrane, post-translational modification, X-ray structure.

- In humans and plants, N-terminal acetylation plays a central role in protein homeostasis, affects 80% of proteins in the cytoplasm and is catalyzed by five ribosome-associated N-acetyltransferases (NatA–E). Humans also possess a Golgi-associated NatF (*HsNAA60*) that is essential for Golgi integrity. Remarkably, NAA60 is absent in fungi and has not been identified in plants.
- Here we identify and characterize the first plasma membrane-anchored post-translationally acting N-acetyltransferase *AtNAA60* in the reference plant *Arabidopsis thaliana* by the combined application of reverse genetics, global proteomics, live-cell imaging, microscale thermophoresis, circular dichroism spectroscopy, nano-differential scanning fluorometry, intrinsic tryptophan fluorescence and X-ray crystallography.
- We demonstrate that *AtNAA60*, like *HsNAA60*, is membrane-localized *in vivo* by an α -helical membrane anchor at its C-terminus, but in contrast to *HsNAA60*, *AtNAA60* localizes to the plasma membrane. The *AtNAA60* crystal structure provides insights into substrate-binding, the broad substrate specificity and the catalytic mechanism probed by structure-based mutagenesis. Characterization of the NAA60 loss-of-function mutants (*naa60-1* and *naa60-2*) uncovers a plasma membrane-localized substrate of *AtNAA60* and the importance of NAA60 during high salt stress.
- Our findings provide evidence for the plant-specific evolution of a plasma membrane-anchored N-acetyltransferase that is vital for adaptation to stress.

Introduction

Co- and post-translational modifications of proteins contribute significantly to the dynamic alteration of the proteome upon diverse environmental stimuli. Together with alternative splicing events these modifications create millions of distinct proteoforms in human cells, although the human genome contains only about 20 000 protein-coding genes (Ponomarenko *et al.*, 2016). One of the most-abundant protein modifications in higher eukaryotes is N-terminal acetylation (NTA). It plays a vital role in protein–protein interaction, folding, aggregation, localization and stability of the modified proteins (Arnesen, 2011; Linster & Wirtz, 2018). NTA is a highly dynamic process and is regulated upon cellular stress (Gibbs, 2015; Linster *et al.*, 2015; Aksnes *et al.*, 2016). The involvement of NTA in cancer, neurodegenerative diseases and blood vessel formation

provides further evidence for its functional relevance in human metabolism and development (reviewed by Drazic *et al.*, 2016).

NTA is executed co-translationally or post-translationally by N^α-terminal acetyltransferases (Nats) and affects up to 80% of soluble proteins in humans. The vast majority of N-terminally acetylated proteins are imprinted co-translationally by five ribosome-associated Nats (NatA–E). NatA–C are composed of one catalytic subunit and up to two auxiliary subunits, whereas NatD comprises only one catalytic subunit (Aksnes *et al.*, 2019). The NatA complex can also associate with the auxiliary subunit HypK and an additional catalytic subunit NAA50. In the latter case, the complex of NatA and NAA50 is termed NatE (Gautschi *et al.*, 2003; Weyer *et al.*, 2017; Gottlieb & Marmorstein, 2018; Deng *et al.*, 2019; Armbruster *et al.*, 2020). In higher eukaryotes, post-translational Nats (NatF–NatH) have been identified (Aksnes *et al.*, 2015b; Dinh *et al.*,

*These authors contributed equally to this work.

2015; Drazic *et al.*, 2018). The deletion of distinct Nats leads to different phenotypes and often causes fatal errors (Aksnes *et al.*, 2015c). For instance, an NAA60 (NatF) knockdown in human induces Golgi fragmentation and an NAA60 depletion in *Drosophila* exhibits chromosomal segregation defects (Van Damme *et al.*, 2011b; Aksnes *et al.*, 2015b). In humans, NAA60 is anchored to the Golgi apparatus via two C-terminal α -helices and is dedicated to acetylate post-translationally the N-termini of membrane-associated proteins with a broad substrate specificity (Aksnes *et al.*, 2017). Crystal structures of *Hs*NAA60 have been reported, revealing an additional $\beta 6'$ - $\beta 7'$ hairpin, which is involved in the dimer to monomer transition upon substrate binding (Chen *et al.*, 2016; Stove *et al.*, 2016). Of note, *Hs*NAA60 has been reported to have a bi-functional Nat and Kat (Lys-acetyltransferase) activity (Yang *et al.*, 2011; Chen *et al.*, 2016). The human cytosolic NatH has a narrow substrate specificity and acetylates a few processed actin isoforms in a post-translational manner (Drazic *et al.*, 2018). In plants, seven acetyltransferases possessing dual Nat/Kat activity, including NatG, are located in chloroplasts, where NatG post-translationally acetylates N-termini of imported proteins with a broad substrate specificity (Dinh *et al.*, 2015; Bienvenut *et al.*, 2020).

Plants are sessile organisms that must cope with environmental challenges on site. The key for many environmental stress responses is to shape the proteome by stress-induced protein-modification systems. In plants, NTA also occurs in a co-translational manner and affects the majority of cytosolic proteins. The substrate specificity and subunit composition for the ribosome-associated major Nats, NatA and NatB, are conserved in yeast, humans and the reference plant *Arabidopsis thaliana* (Rathore *et al.*, 2016; Linster & Wirtz, 2018; Huber *et al.*, 2020). The essential plant NatA complex is dynamically regulated by the stress-related phytohormone ABA and tunes the drought stress response (Linster *et al.*, 2015). Also, the immune response towards the pathogen *Pseudomonas syringae* pv *maculicola* 1 is controlled by N-terminal protein acetylation. In this case, NatA and NatB team up to control the protein stability of two proteoforms of the Nod-like receptor SNC1 with different N-termini (Xu *et al.*, 2015). These findings led to the hypothesis that hormone-induced modification of the N-acetyloyme might regulate diverse stress responses in plants (Linster & Wirtz, 2018; Aksnes *et al.*, 2019). In addition, we demonstrated that depletion of NatB in *A. thaliana* increases the plant sensitivity towards osmotic and high-salt stress (Huber *et al.*, 2020).

As an NAA60 ortholog has been suggested in plants (Van Damme *et al.*, 2011b; Rathore *et al.*, 2016), we set out to investigate if a membrane-associated NAA60 is present in photosynthetically active eukaryotes and to analyze its structure and function. In this study, we show that *At*NAA60 is localized at the plasma membrane and acetylates a membrane-bound substrate. The *At*NAA60 structure reveals its substrate-binding mode and catalytic mechanism and we demonstrate that NAA60 affects the plants' response towards protein-harming stress such as high salinity.

Materials and Methods

Plant material and growth conditions

All analyses were carried out on *A. thaliana* plants from the ecotype Col-0. The T-DNA insertion lines for *At*NAA60, *naa60-1* (SALK_016406C) and *naa60-2* (WiscDsLoxHs132_03H) belong to the SALK and the Wisconsin collection, respectively, and were obtained from the Nottingham Arabidopsis Stock centre (NASC). Transformation of *Agrobacterium tumefaciens* GV3101 with binary vectors and subsequent stable transformation and selection of *Arabidopsis thaliana* Col-0 was performed according to Clough & Bent (1998). Arabidopsis plants were grown in climate chambers on growth medium containing one-half soil and one-half substrate 2 (Klasmann-Deilmann, Geeste, Germany) or on 1 × MS (Murashige Skoog) medium under sterile conditions at 8.5 h light, 100 μ mol light photon flux density, 22°C at day, 18°C at night and 50% humidity.

PCR

PCR for identification of T-DNA insertion lines was performed with the FastGene Taq 2 × Ready Mix from Nippon Genetics. Genotyping of *naa60-1* was conducted with specific primers for the wild type allele (Gen_AtNAA60_LP, Gen_AtNAA60_RP) and mutant allele (Gen_SALK-LB1.3n). For cloning, DNA was amplified with the PCR BIO HiFi Polymerase (PCR Biosystems, London, UK). In both cases, the PCRs were performed according to the supplier's instructions. Primer sequences are listed in Supporting Information Table S1.

qRT-PCR

Total RNA was extracted from leaf tissue with the peqGOLD total RNA Kit (Peqlab, Erlangen, Germany) according to the manufacturer's protocol. Total RNA was subsequently transcribed into complementary DNA using the RevertAid H minus first-strand cDNA synthesis Kit (Thermo Fisher, Waltham, MA, USA) and analyzed by quantitative reverse transcriptase PCR (qRT-PCR) using qPCR BIO SyGreen Mix Lo-ROX (PCR Biosystems). Data were analyzed with the Rotor-Gene Q Series Software (Qiagen, Hilden, Germany). Primer sequences are listed in Table S1.

Cloning

For recombinant expression of *At*NAA60, a full-length coding sequence was amplified by PCR from *A. thaliana* cDNA. The PCR fragment was digested with *Nco*I and *Bam*HI and ligated into the corresponding sites of pET24d (Novagen) or in pETM41 (N-terminal His/MBP-fusion). *At*NAA60₂₀₋₂₀₀ truncation variant sequence was PCR-amplified using *At*NAA60-pET24d as template, digested and ligated into the pETSUMO vector (G. Stier, Heidelberg, Germany) digested *Nco*I and *Bam*HI, resulting in His₆-TEV (tobacco etch virus cleavage sequence)-SUMO (small ubiquitin-like modifier 1a) fused to *At*NAA60₂₀₋₂₀₀. For localization of *At*NAA60-YFP, CFP-

AtNAA60, GFP-*AtNAA60*₁₋₂₀₆ or CFP-*AtNAA60*₂₀₇₋₂₇₀, *AtNAA60* was PCR amplified by using the NAA60-start_YFP_f, NAA60-end_YFP_rev, NAA60-start_f, NAA60-end_r, NAA60-start_f, NAA60-Nterm_r, NAA60-cterm_f and NAA60-end_r primers and cloned via Gateway technology (Invitrogen) in the binary vectors pB7YWG2.0 (C-terminal YFP), pB7WGC2 (N-terminal CFP) or pK7WGF2 (N-terminal GFP). All constructs were verified by DNA sequencing. Primer sequences are listed in Table S1.

Protein purification, crystallization, data collection and structure determination

Protein purification, crystallization and data collection strategies are described in Methods S1 and S2.

Multi-angle light scattering (MALS)

*AtNAA60*₂₀₋₂₀₀ (0.1 mg) was incubated with AcCoA in a 1:1 molar ratio and injected onto a Superdex 75 10/300 gel-filtration column (GE Healthcare, Little Chalfont, UK) in buffer G. The column was connected to a MALS system (Daw Heleos II 8+ and Optilab T-rEX, Wyatt Technology, Santa Barbara, CA, USA). Data were analyzed using the Astra 6 software (Wyatt Technology).

Analytical size exclusion chromatography (SEC)

For analytical SEC measurements, *AtNAA60*₂₀₋₂₀₀ was incubated with AcCoA, CoA or CoA-Ac-MVNAL in various molar ratios (1 : 1, 1 : 3 or 1 : 10) and the samples were loaded on a Superdex 75 10/300 gel-filtration column (GE Healthcare) equilibrated in buffer G. The peak fractions were analyzed by Coomassie-stained SDS-PAGE gel.

In vitro acetyltransferase assays

For determination of the substrate binding affinity, the acetylation activity of *AtNAA60* and variants was determined using a microplate assay (Skaff & Miziorko, 2010) with the modifications as described in Methods S3. Enzymatic activity on selected peptides was independently confirmed with an assay based on radioactively labeled acetyl-Coenzyme A (Methods S4). For comparison of Nat and Kat activity, the acetyltransferase activity assay was performed as described by Koskela *et al.* (2018) with minor modifications (Methods S5).

Global acetylome profiling (GAP) assay

To analyze the substrate specificity of the *AtNAA60*₂₀₋₂₀₀ protein, *AtNAA60*₂₀₋₂₀₀ was fused with a SUMO Tag (see Cloning) and expressed for 5 h in the Rosetta II (*DE3*) *Escherichia coli* cells (Novagen) at 37°C. Extraction of *E. coli* proteins and analysis of the N-terminal acetylome were performed as described by Dinh *et al.* (2015). The resulting MS data have been deposited in the

PRIDE archive (<https://www.ebi.ac.uk/pride>, Project: PXD016533).

Protein N-terminal characterization and N-terminal acetylation quantification

Soluble leaf proteins from 6-wk-old soil-grown wild type and the *NAA60*-depleted mutants were extracted for protein N-terminal characterization and quantification of N-terminal acetylation. The extracted proteins were processed and enriched by an SCX approach for quantification of N-terminal peptides using MS as described by Bienvenu *et al.* (2017). The resulting MS data have been deposited in the PRIDE archive (<https://www.ebi.ac.uk/pride>, Project: PXD016494).

Localization of *AtNAA60* in *A. thaliana* protoplasts or in *N. benthamiana* leaves

The isolation and transfection of mesophyll protoplasts from *Arabidopsis* were performed as described by Sparkes *et al.* (2006). Agrofiltration of *Nicotiana benthamiana* was done as described by Yoo *et al.* (2007). Protoplasts and tobacco leaves were imaged 2 d after transfection using a Nikon A1R confocal laser-scanning microscope. The fluorescence intensities were collected at 482/35 nm after excitation with 445 nm for cyan fluorescent protein (CFP) and mTq2, 515/30 nm after excitation with 514 nm for yellow fluorescent protein (YFP), 525/50 nm after excitation at 488 nm for green fluorescent protein (GFP) and 700/75 nm after excitation with 640 nm for the chlorophyll autofluorescence. For visualization of the nucleus, nuclear DNA was stained by leaf infiltration of 0.3 µM DAPI for 10 min and imaged at 450/50 nm after excitation at 405 nm. To stain the plasma membrane, tobacco leaf disks were floating on ddH₂O supplemented with 10 µM MM46-4 (Santa Cruz Biotechnology, Santa Cruz, CA, USA). After 20 min of incubation, leaves were rinsed in ddH₂O and imaged at 595/50 nm after excitation at 561 nm. As localization marker for the Golgi apparatus, SYP32-mCherry (wave22r, Geldner *et al.*, 2009) and AtXylT-mTq2 (pDOE10, Gookin & Assmann, 2014) were used. The mVenus fluorophore from pDOE10 was replaced by 140 bp of the pJet1.2 backbone (Thermo Fisher Scientific) using the primers pJet_backbone_amplif_for and pJet_backbone_amplif_rev. Primer sequences are listed in Table S1.

Biochemical characterization of *AtNAA60*

The physicochemical properties of *AtNAA60* were determined by NanoDSF, microscale thermophoresis, intrinsic tryptophan fluorescence, circular dichroism spectroscopy, preparation of plasma membrane-like liposomes and *in vitro* inhibition assays with the bisubstrate analog CoA-Ac-MVNAL. Detailed description of these diverse assays is provided in Methods S6–S12. The bisubstrate analog CoA-Ac-MVNAL synthesis was based on Foyn *et al.* (2013) with slight modifications. In brief, the MVNAL peptide was mixed with bromoacetic acid and *N,N*-diisopropylcarbodiimide (DIC) to obtain a bromo-acetylated

peptide. Subsequently, coenzyme A was added in an aqueous buffer to yield CoA-Ac-MVNAL.

Electron microscopy

Electron microscopy was performed at the EM Core Facility of Heidelberg University as outlined in Methods S13.

NaCl stress germination assay

To study the involvement of NAA60 in salt stress response, seeds of wild type, *naa60-1* and two *naa60-1/AtNAA60-YFP* lines were surface sterilized with 70% ethanol. The seeds germinated under short-day conditions after 2 d of stratification at 4°C on 1× MS medium (Duchefa), 1% (w/v) sucrose, 0.4 g l⁻¹ MES, 0.6% micro agar (Duchefa, Amsterdam, the Netherlands) and 120 mM NaCl. Seed germination, emergence of the radicle, was monitored every 2 d and pictures were taken 1 and 2 wk after stratification.

Results

Identification and subcellular localization of AtNAA60

So far, a membrane-associated N-terminal acetyltransferase has not been reported in plants. Therefore, we used the human NAA60 protein sequence in a BLAST search to predict an orthologous protein in *A. thaliana* (Table S2). This search revealed one candidate, encoded by At5g16800, which shows 27% amino acid sequence identity with the human NAA60 and important residues for catalytic activity are conserved with other Nats (NAA50, NAA20 and NAA10) (Fig. S1a). Transcription of At5g16800 was verified in rosette leaves, cauline leaves, stem and flowers by qRT-PCR (Fig. S1b). Recombinant full-length HisMBP-At5g16800 was tested for N-terminal protein acetylation and displayed activity on the canonical human NAA60 substrate MVNA *in vitro* (Fig. 1a). The hallmark of human NAA60 is its association with membranes and in particular with the Golgi apparatus. Ultracentrifugation combined with immunological detection revealed that transiently expressed full-length At5g16800 in fusion with YFP at its C-terminus (At5g16800-YFP) also localizes to membranes (Fig. 1b). Next, we applied confocal imaging to unravel in which membrane system AtNAA60 localizes *in planta*. Transient expression of the full-length At5g16800 protein in fusion with CFP at its N-terminus (CFP-At5g16800) or At5g16800-YFP resulted in specific localization of the protein at the plasma membrane in tobacco leaf pavement cells or in Arabidopsis leaf protoplasts (Figs 1c, S2). No obvious co-localization of At5g16800-YFP or CFP-At5g16800 with the Golgi markers, AtXylt-mTq2 and SYP32-mCherry, could be observed in tobacco leaves or in Arabidopsis protoplasts (Fig. 1i–k, At5g16800-YFP; Fig. S2A–D, CFP-At5g16800). Based on the membrane-localization and its acetylation activity on protein N^ε-termini we specified the identity of At5g16800 as AtNAA60. A protein sequence alignment of AtNAA60 with putative homologs from other plant species

suggests the conservation of NAA60 across the plant kingdom (Fig. S3).

Characterization of AtNAA60 enzymatic activity and specificity *in vitro* and *in vivo*

Because purified recombinant untagged full-length AtNAA60 was poorly soluble and was prone to aggregation, we cloned and expressed various truncated variants of AtNAA60 for enzymatic characterization in *in vitro* acetylation assays. Only the truncated AtNAA60₂₀₋₂₀₀ variant was stable and could be purified to homogeneity (Fig. S4a,b). We first tested AtNAA60 substrate selectivity using five peptides identified as substrates for NatA (SESS, Arnesen *et al.*, 2009), NAA10/NAA80 (EEEI, Van Damme *et al.*, 2011a; Drazic *et al.*, 2018), NatB (MDEL, Starheim *et al.*, 2008) and NatC/E/F (MLGTE and MVNALE, Van Damme *et al.*, 2011b). In agreement with results for full-length HisMBP-AtNAA60, the truncated AtNAA60₂₀₋₂₀₀ showed acetylation activity towards the peptides MLGTE and MVNALE and no activity towards the others (Fig. 2a). The highest acetylation efficiency was detected for the MVNALE peptide, which was then used for the determination of the enzymatic parameters. AtNAA60 shows a Michaelis–Menten constant (K_m) towards acetyl-CoA of $43.7 \pm 8.4 \mu\text{M}$ and a turnover rate (k_{cat}) of $36.4 \pm 2.0 \text{ min}^{-1}$ (Fig. S4c), which is in the same range (24–59 μM) as the K_m of NatA (Liszczak *et al.*, 2013; Weyer *et al.*, 2017), NatB (Hong *et al.*, 2017; Huber *et al.*, 2020) and Naa50 (Liszczak *et al.*, 2013). To validate the results of the *in vitro* acetylation assays, we determined the substrate specificity of AtNAA60 by applying the previously established *in vivo* GAP assay (Dinh *et al.*, 2015). In the GAP assay, several hundred N-termini from bacterial proteins were offered in a competitive manner to the recombinant AtNAA60₂₀₋₂₀₀ variant. Based on the quantified acetylation level of the N-termini characterized by MS, 66 N^ε-termini were acetylated specifically after expression of AtNAA60₂₀₋₂₀₀ (Table S3). Of these N-termini, 58 start with the iMet. The web logo of these substrates reveals that position 2 is highly variable (Fig. 2b). Furthermore, eight identified substrates of AtNAA60 (10%) were subject to iMet excision before acetylation (Fig. 2c). Seven of these substrates displayed an Ala N-terminus. However, an AA-starting peptide was not acetylated *in vitro* (Fig. 2a). The broad substrate specificity identified here agrees with the observed substrate spectrum of the human NAA60 (Van Damme *et al.*, 2011b; Aksnes *et al.*, 2015b).

As human NAA60 is a bi-functional enzyme that also exhibits Kat activity (Yang *et al.*, 2011; Chen *et al.*, 2016), we tested whether this holds true also for AtNAA60. To compare the Nat and the N^ε-Kat activities of AtNAA60₂₀₋₂₀₀, we used specific synthetic peptide substrates, which have an identical amino acid sequence (AAK(2-aminobenzoyl)GAK(ac)AAK(2,4-dinitrophenyl)-6-aminohexanoic acid-rrr and A(ac)AK(2-aminobenzoyl)GAKAAK(2,4-dinitrophenyl)-6-aminohexanoic acid-rrr (r = D-arginine). The peptide substrate for the Nat assay has a free alpha amino group at the N-terminus and an acetylated lysine side chain, while the peptide for the Kat assay has a free epsilon amino group at the lysine side chain and an acetylated

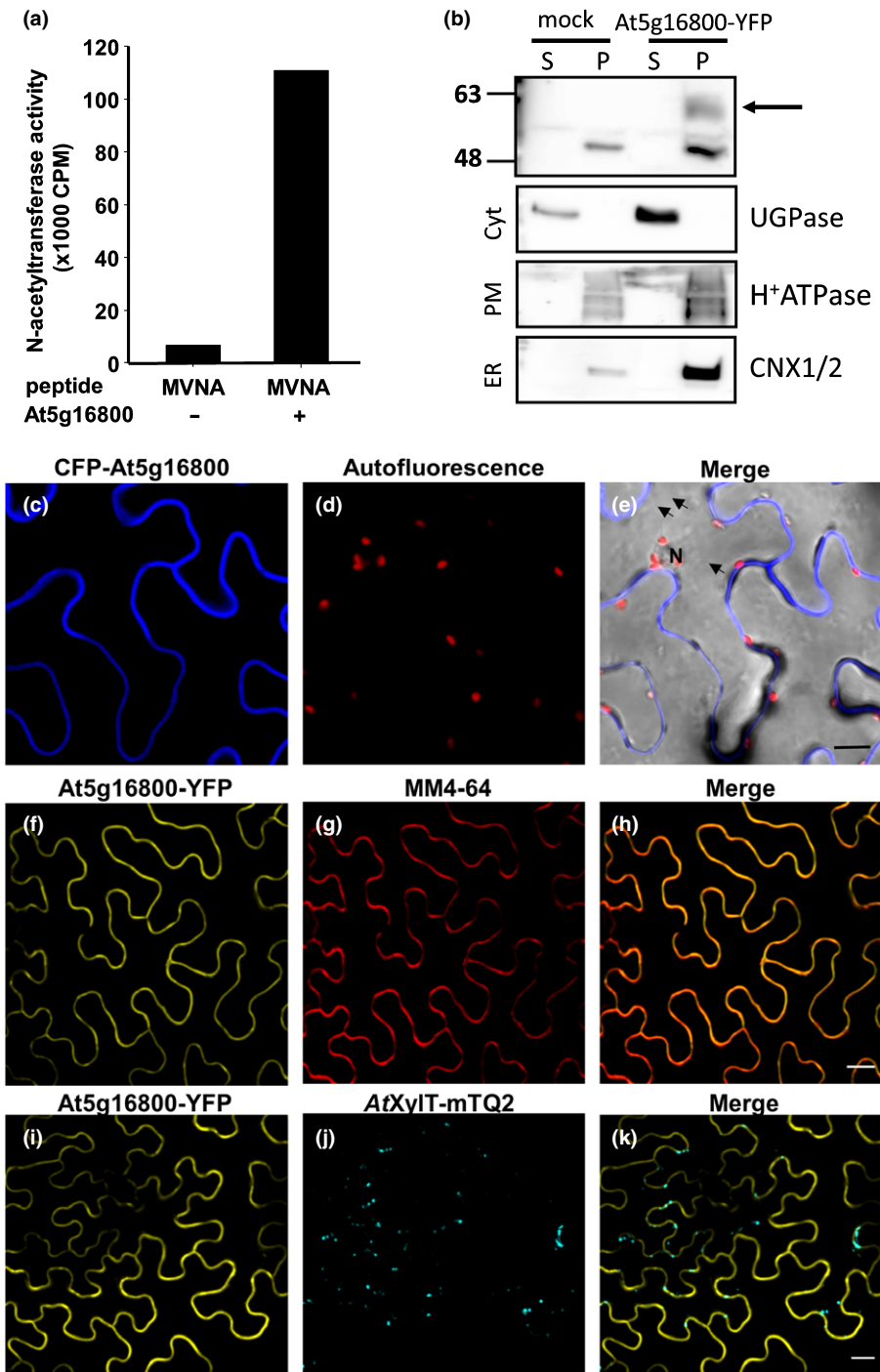


Fig. 1 N-terminal acetyltransferase activity and subcellular localization of At5g16800. (a) *In vitro* N-terminal acetylation activity of full-length HisMBP-At5g16800 tested with MVNA peptide (NatC/E/F substrate), $n = 1$. (b) Fractionation of untransformed *Nicotiana benthamiana* leaf cells (mock) and cells transiently expressing At5g16800-YFP into supernatant (S) and pellet (P) by differential ultracentrifugation. The At5g16800-YFP fusion protein was immunologically detected using a polyclonal GFP-specific antiserum (A-6455; Thermo Fisher Scientific, black arrow). Immunological detection of the marker proteins UGPase (UDP-glucose pyrophosphorylase; AS05086; Agrisera, Vännäs, Sweden), plasma membrane H⁺ATPase (AS07260; Agrisera) and CNX1/2 (CALNEXIN HOMOLOG 1/2, AS122365; Agrisera) was used to identify fractions corresponding to the cytosol (Cyt; 2nd panel), the plasma membrane (PM; 3rd panel) and the endoplasmic reticulum (ER; lower panel) respectively. (c–k) Subcellular localization study of full-length At5g16800 in fusion with CFP (c–e) or YFP (f–k) in *N. benthamiana*. (c) CFP-At5g16800 signal in pavement cells. (d) Autofluorescence of the chloroplasts. (e) Merge of both signals in the bright field image of *N. benthamiana* pavement cells. (f, i) At5g16800-YFP signal in two independently transformed *N. benthamiana* leaves. (g) Staining of the cells shown in (f) with the plasma membrane-specific dye MM4-64. (h) Merge of the At5g16800-YFP (f) and the plasma membrane signal (g). (j) Detection of the Golgi marker AtXylt-mTQ2 in the CFP channel of cells shown in (i). (k) Overlay of the At5g16800-YFP-specific signal (i) and the Golgi-marker (j). Cytosol and nucleus are marked with black arrows and N in (e), respectively. Bars, 20 μ m.

N-terminus. The N^α-terminal acetylation rate was around 450-fold higher than the N^ε-Lys acetylation rate, indicating AtNAA60 Nat activity is higher than its Kat activity for the tested peptides (Fig. 2d).

Structural characterization of AtNAA60

To characterize AtNAA60 at the atomic level, AtNAA60_{20–200} was crystallized in complex with AcCoA (AtNAA60/AcCoA) and in complex with the bisubstrate analog CoA-Ac-MVNAL

(Fig. S5a) (AtNAA60/CoA-MV). The design of the bisubstrate was based on the most effectively acetylated substrate MVNALE (Fig. 2a). For both complexes, well-diffracting crystals in space group P 2₁ 2₁ 2₁ with two NAA60 molecules per asymmetric unit but with different cell dimensions could be obtained. Initial phases for the AtNAA60/AcCoA complex were obtained by molecular replacement with the HsNAA60/CoA-MK structure (Stove *et al.*, 2016). The AtNAA60/CoA-MV data set was phased using AtNAA60/AcCoA as the molecular replacement search model. Subsequently, X-ray structures could be built at 1.75 Å

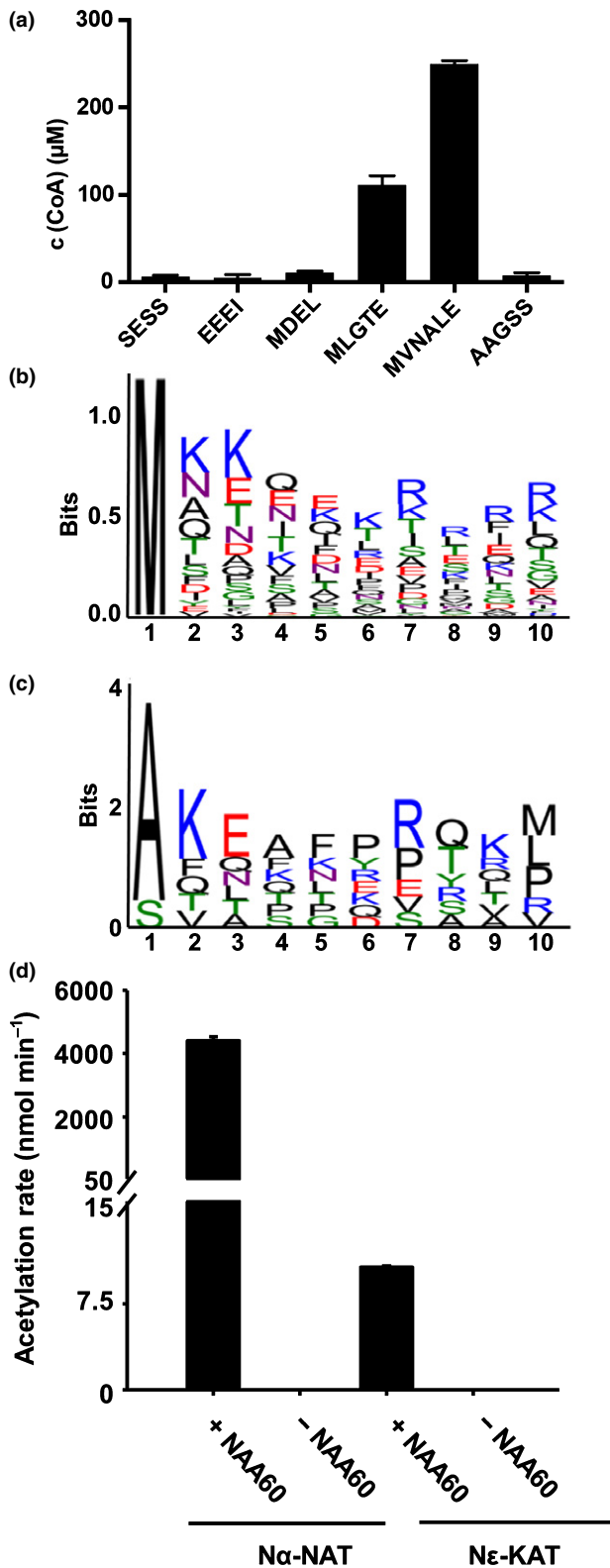


Fig. 2 Substrate specificity of *AtNAA60*. (a) Substrate specificity of *AtNAA60*₂₀₋₂₀₀ tested *in vitro* with six different peptides. The peptides SESS, EEEL, MDEL, MLGTE and MVNALE were previously identified as NatA, Naa10/Naa80, NatB and NatC/E/F substrates. Data represent mean \pm SD ($n = 3$). c, concentration. (b, c) Global acetylome profiling (GAP) assay of *AtNAA60* in *Escherichia coli*. Web logos of N-termini from *E. coli* proteins specifically acetylated at the initiator methionine (iMet) (b) or at the second last amino acid after iMet excision (c), after expression of *AtNAA60* in *E. coli* ($n = 2-3$). Amino acids are colored according to their chemical properties: polar amino acids (green), basic (blue), acid (red) and hydrophobic amino acids (black). (d) HPLC-based *in vitro* analysis of the N^ε-terminus and N^ε-Lys acetylation catalyzed by *AtNAA60*. The conversion rate as defined in the Material and Methods section was normalized to 1 μ M NAA60 (+NAA60). The assay approach lacking the enzyme was applied as a control (-NAA60, $n = 3$ technical replicates). Data represent mean \pm SE.

For *AtNAA60*/CoA-MV, the structure is complete for residues 24–200 and contains a bisubstrate analog with the peptide sequence M1_pV2_pN3_pA4_p (Fig. 3a). The root mean square deviation (rmsd; C α) between the two *AtNAA60*/CoA-MV complexes is 0.64 Å (i.e. both molecules have very similar overall conformation). Loop α 1– α 2 and hairpin β 6'– β 7' fold over part of the substrate binding site and are in direct van-der-Waals contact. The sidechain of residue M1_p is positioned in a hydrophobic pocket formed by residues F46, P47, I48 (loop α 1– α 2), I156 (β 5) and Y181 (hairpin β 6'– β 7') (Fig. 3b). Additionally, there are distinct interactions between the substrate peptide main chain and the protein. The M1_p amide nitrogen and carbonyl oxygen form hydrogen bonds to the carbonyl oxygen of H154 and the sidechain of Y181, and V2_p forms hydrogen-bonds via its amide and carbonyl groups to the L117 backbone carbonyl and the Y50 sidechain, respectively. The N3_p sidechain amino group engages in a polar contact to the F180 backbone carbonyl (Fig. S5c). A4_p is not involved in intermolecular interactions and no electron density could be attributed to L5_p. In summary, residues 1 and 2 of the bound inhibitor show specific interactions with the active site, and the structure suggests high selectivity for methionine in position 1 as it perfectly matches the hydrophobic binding pocket.

For *AtNAA60*/AcCoA, the structure is complete for residues 24–199 and contains AcCoA (Fig. S5b). The rmsd(C α) between the two protein chains A and B in the asymmetric unit is 1.23 Å. This indicates a higher local flexibility of *AtNAA60*/AcCoA compared to the *AtNAA60*/CoA-MV complex.

Structural determinants of the catalytic mechanism and substrate specificity

NTA by Nats is generally carried out via base catalysis (Liszczak *et al.*, 2011). In *AtNAA60* a water molecule is present in the active site, which is probably involved in the deprotonation of the target amine. This catalytically important water is coordinated by the Y115 hydroxyl group, the H154 backbone amide nitrogen, the I116 carbonyl oxygen and the target M1_p nitrogen (Fig. 3c). Of note, the arrangement of the active site residues and the catalytic water are similar to the *HsNAA60* structures (Stove *et al.*, 2016; Chen *et al.*, 2016). The substrate specificity of *AtNAA60* for N-termini containing the initiator methionine can

for *AtNAA60*/AcCoA and 1.77 Å for *AtNAA60*/CoA-MV (Table S4). Both structures show the characteristic Gcn5-related N-acetyltransferase (GNAT) fold (Vetting *et al.*, 2005) with six β -strands and four α -helices and a central AcCoA- and substrate-binding site (Fig. S5b).

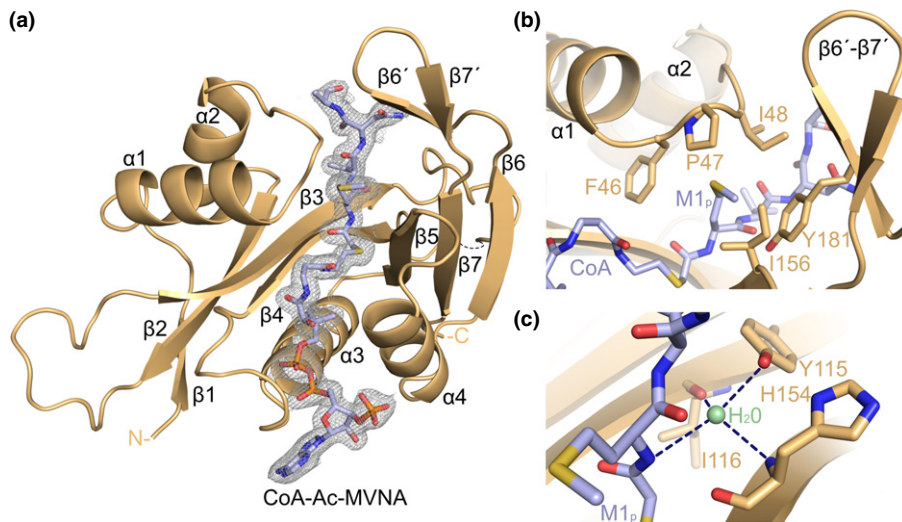


Fig. 3 Structure of the AtNAA60/CoA-MV complex. (a) AtNAA60 is shown in light brown and the bisubstrate analog is shown as blue sticks with nitrogen, oxygen, phosphorus and sulfur shown in blue, red, orange and yellow, respectively. The 2mFobs-DFcal electron density around the bisubstrate is shown at a contour level of 1 σ (gray mesh). (b) The sidechain of M1_p is positioned in a hydrophobic pocket formed by residues F46, P47, I48, I156 and Y181. (c) The catalytically important water (green) is coordinated by Y115, the backbone of H154 and I116 and the target nitrogen of M1_p. Dashed lines represent hydrogen bonds.

be explained by the multiple interactions of M1_p with the residues forming the hydrophobic pocket. Upon peptide binding the hydrophobic residues F46, P47, I48 and I156 rearrange to accommodate M1_p (Fig. S5d). Smaller sidechains such as alanine or serine would spatially fit in this pocket, rationalizing the acetylation of alanine residues in the GAP assay (Fig. 2c). However, forming fewer hydrophobic interactions than M1_p, the A1_p (of the AAGSS peptide) was not acetylated *in vitro* (Fig. 2a). At the second position of the substrate there is enough space for amino acids with bulkier sidechains. Together, the structure visualizes the observed substrate specificity.

To further characterize NAA60 kinetics and substrate binding, the novel bisubstrate CoA-Ac-MVNAL was probed for its impact on NAA60 catalytic activity. This bisubstrate analog is a potent competitive inhibitor of NAA60 with a half-maximum inhibitor concentration (IC₅₀) of 2.3 ± 1.2 μM and a K_i of 0.32 ± 0.06 μM (Fig. S6a). Microscale thermophoresis experiments showed that CoA-Ac-MVNAL binds tightly to NAA60 with a dissociation constant (K_d) of 26.4 ± 7.1 nM (Fig. S6a). Furthermore, the effect of CoA-Ac-MVNAL on the stability of NAA60 was investigated using nano-differential scanning fluorimetry (nanoDSF). NAA60 showed an unfolding transition temperature of 54°C, shifting to 76°C when the bisubstrate analog was added in 2 molar fold excess. Notably, the shape of the first derivative of the thermal unfolding curve was narrowing upon inhibitor addition, indicating that the inhibitor limits NAA60 flexibility (Fig. S6a).

Characterization of AtNAA60 enzymatic mechanism

The importance of specific residues on acetylation efficiency was then examined using structure-based mutagenesis studies. Various single mutations in the active site (Y115A, Y181A, H154A/F) and substrate binding pocket (F46A, P47A, I48A, Y50A, F180A) were tested. Mutations in the active site impaired acetylation, whereas mutations in the substrate binding pocket showed a milder decrease of acetylation efficiency. These results confirm

the critical role of these residues for the enzymatic mechanism (Table 1). As expected, the F46A mutation has a strong effect on NAA60 catalytic efficiency, as it contacts the M1_p and its corresponding residue F34 in human was also shown to position the AcCoA (Chen *et al.*, 2016). The influence of the H154A/F mutation is difficult to quantify, as these mutations lead to destabilization of the protein, as shown by nanoDSF (Fig. S6b). The structure demonstrates that the replacement of H154 by an A or F would abolish the hydrogen bonds to E97 of loop β3–β4 and to the Y115 sidechain, leading to the destabilization of the protein (Fig. S6c). However, when E97 is mutated to an alanine, abolishing the hydrogen bond with H154, protein stability is only mildly affected, and the catalytic efficiency is decreased by 20% compared to the wild type. The Y115A and Y181A mutants are catalytically defective as the Y115A mutation impairs the coordination of a water molecule essential for the catalysis and the Y181A mutation breaks the hydrogen bond with the M1_p main chain carbonyl.

Table 1 Catalytic efficiency of SUMO-AtNaa60₂₀₋₂₀₀ (SUMO-WT) and mutants.

Enzyme	k _{cat} (min ⁻¹)	K _m (μM)	Wild type efficiency (%)
SUMO-WT	49.2 ± 3.6	60.6 ± 15.2	100.0 ± 25.9
F46A	0.3 ± 0.3	28.4 ± 29.7	1.2 ± 1.3
P47A	10.2 ± 0.4	34.5 ± 4.8	36.5 ± 5.3
I48A	3.3 ± 0.1	8.8 ± 1.9	46.4 ± 10.1
Y50A	25.7 ± 2.4	25.7 ± 2.4	68.3 ± 16.1
E97A	32.2 ± 1.4	46.5 ± 10.7	72.5 ± 11.4
Y115A	0.2 ± 0.1	20.5 ± 10.0	1.0 ± 0.8
H154A	nd	nd	nd
H154F	nd	nd	nd
F180A	13.0 ± 0.6	5.7 ± 2.1	280.7 ± 104.1
Y181A	0.4 ± 0.1	1.8 ± 7.7	1.5 ± 1.6
AtNAA60 ₂₀₋₂₀₀ (WT)	36.4 ± 2.0	43.7 ± 8.4	102.5 ± 21.0

The wild type efficiency is based on the k_{cat}/K_m value and normalized to SUMO-WT. nd, not determined. Error values represent SD (n = 3).

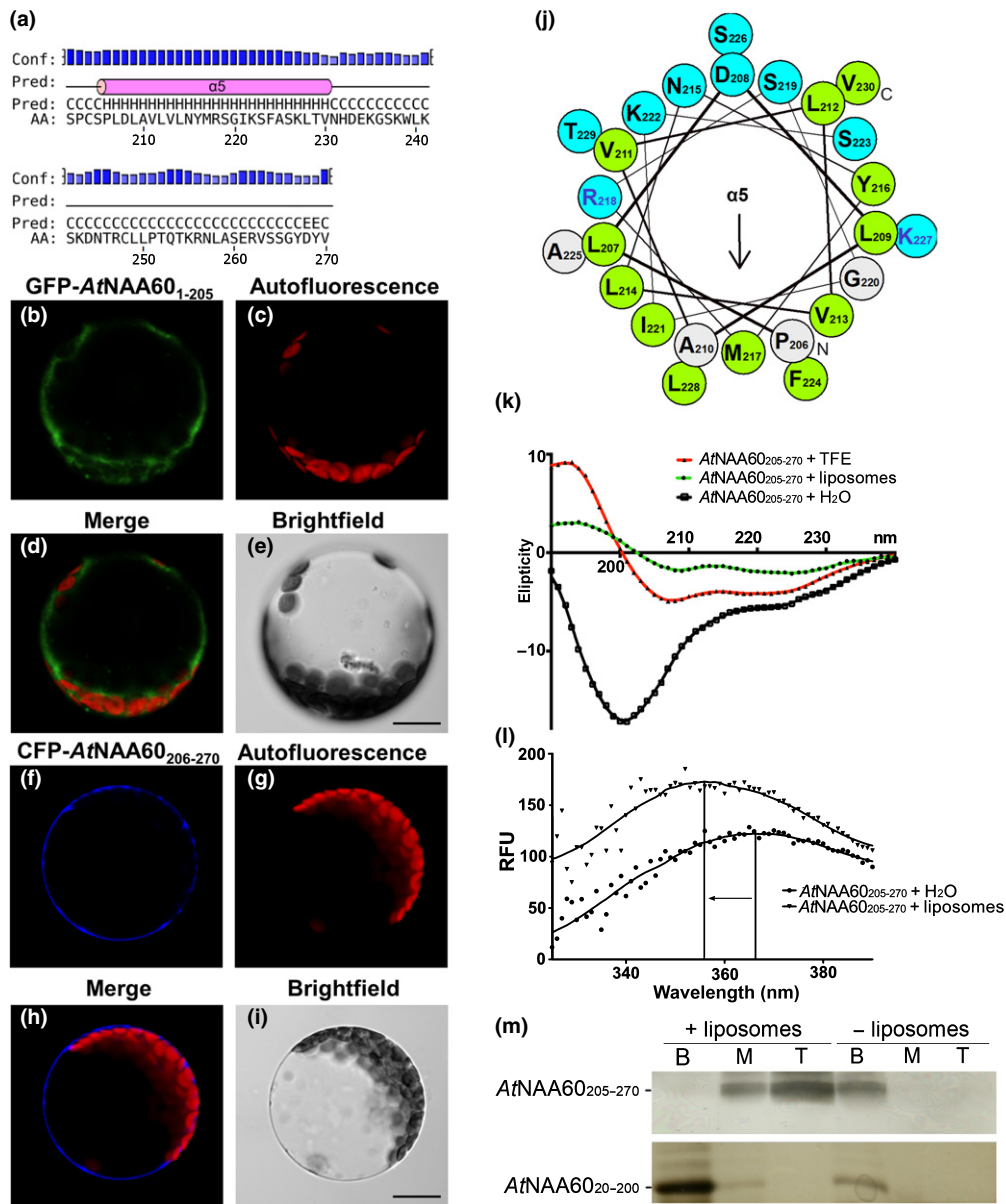
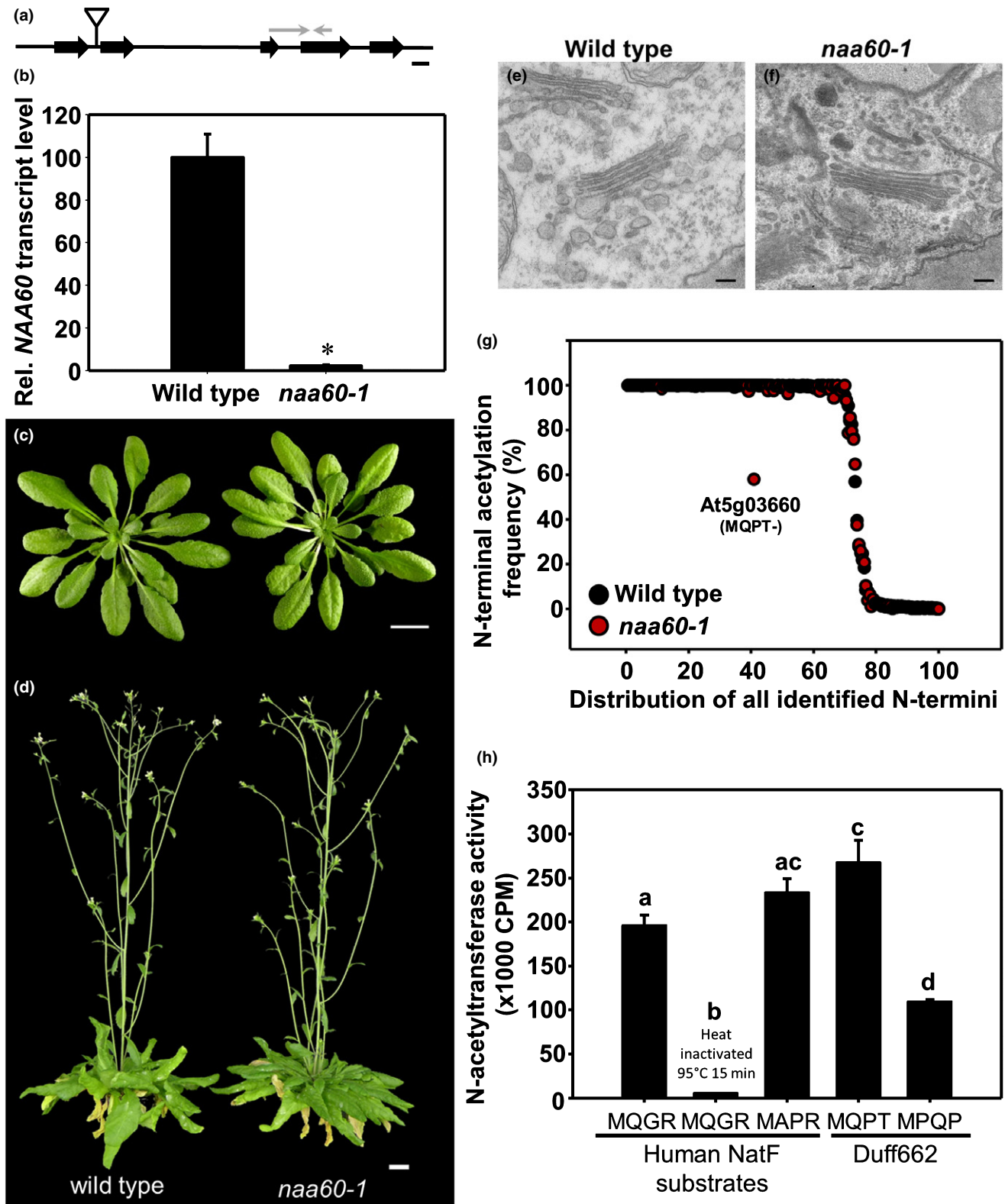


Fig. 4 Contribution of the *AtNAA60* C-terminus to subcellular localization. (a) The secondary structure prediction of the *AtNAA60* C-terminus was done with the PSIPRED server (Buchan & Jones, 2019) and shows the predicted $\alpha 5$ (amino acids 206–230). Conf., confident level; Pred, prediction. AA, amino acid. (b–i) Subcellular localization of GFP-*AtNAA60*_{1–205} (b–e) and CFP-*AtNAA60*_{206–270} in *Arabidopsis thaliana* protoplasts (f–i). GFP- (b) and CFP- (f) fluorescence was recorded for localization of GFP-*AtNAA60*_{1–205} or CFP-*AtNAA60*_{206–270}. Chloroplasts were imaged by recording the Chl autofluorescence (c, g). Merge of the fluorescent protein signal and the Chl autofluorescence (d, h). Bright-field image of the corresponding protoplast (e, i). Bars, 10 μm . (j) Helical wheel representation of the predicted $\alpha 5$ -helix with a hydrophobic face on the lower site, a hydrophilic face on the upper site, and residues R218 and K227 at the interface. The arrow indicates the direction of the hydrophobic moment. Hydrophilic, neutral and hydrophobic residues are shown in blue, gray and green, respectively. (k) Circular dichroism spectra of *AtNAA60*_{205–270} dissolved in water, incubated with liposomes or mixed with 78% trifluoroethanol (TFE). (l) Intrinsic tryptophan fluorescence assay of *AtNAA60*_{205–270} in water and with liposomes. The vertical lines and the arrow highlight the fluorescence maxima and the corresponding blue-shift, respectively. RFU = relative fluorescence unit. (m) Liposome flotation assays of *AtNAA60*_{205–270} and *AtNAA60*_{20–200} in the presence (+) and absence (–) of liposomes. Presence of the proteins in the collected fractions (B, M, T) was visualized by silver-staining of SDS-PAGE-separated proteins. B, bottom fraction; M, middle fraction; T, top fraction.

The mutated residues in *AtNAA60* (F46, P47, I48, Y50, Y115, H154 and Y181) are conserved in *HsNAA60* (Fig. S1a) and mutations of the corresponding residues also affected the catalytic activity (Chen *et al.*, 2016; Stove *et al.*, 2016). Overall, these residues play similar roles in catalytic activity in the two organisms, underlining that the structure and enzymatic mechanism in both organisms is conserved.

Oligomeric status of *AtNAA60*_{20–200}

The structure of truncated *AtNAA60* (residues 20 to 200) complexed with AcCoA or CoA-Ac-MVNAL is a monomer, while the corresponding truncated *HsNAA60* variant (residues 5 to 184) was described to form a homodimer when complexed with CoA (Chen *et al.*, 2016; Stove *et al.*, 2016). As *AtNAA60* and



HsNAA60 present a high conservation in structure and mechanism of action, we investigated *AtNAA60* oligomeric status upon incubation with AcCoA, CoA, CoA-Ac-MVNAL or no ligand. Analytical SEC and MALS analysis showed that all *AtNAA60*

complexes are a monomer in solution (Fig. S4a,b). To rationalize this intriguing difference between the human and plant NAA60, we compared *AtNAA60*/CoA-MV and *HsNAA60*/CoA-MK structures. The structures superimpose well (rmsd($C\alpha$) = 1.42 Å),

but with two striking differences. The loop $\beta 2$ – $\beta 3$ is extended in *Arabidopsis* and the loop $\beta 3$ – $\beta 4$ shows a different architecture (Fig. S7a). Importantly, the two *AtNAA60* structures show similar conformations of loop $\alpha 1$ – $\alpha 2$ and hairpin $\beta 6'$ – $\beta 7'$ as *HsNAA60/CoA*-MK, closing over the substrate-binding site. Superposition with *HsNAA60/CoA* shows that positions of hairpin $\beta 6'$ – $\beta 7'$ are dramatically different (Fig. S7b), and only *HsNAA60/CoA* adopts a dimer-forming conformation with hairpin $\beta 6'$ – $\beta 7'$ rotated away from the active site. The dimer interface of *HsNAA60/CoA* is formed by antiparallel interaction of two $\beta 7'$ strands from the two protomers and the interaction of hairpin $\beta 6'$ – $\beta 7'$ with part of the substrate binding pocket of the other protomer (Stove *et al.*, 2016). The sequence of the $\beta 6$ – $\beta 7$ loop region differs between *Hs* and *At* (Fig. S1a), which might explain why *AtNAA60* does not form dimers.

Characterization of the *AtNAA60* plasma-membrane targeting *in planta*

In contrast to *HsNAA60* localizing to the Golgi via two amphipathic helices at the C-terminus (Aksnes *et al.*, 2017), *AtNAA60* associates to the plasma membrane *in planta* (Fig. 1c–h). Because only the truncated *AtNAA60*_{20–200} is soluble and secondary structure prediction of the C-terminal region *AtNAA60*_{202–270} suggests that it contains one α -helix (Fig. 4a), we hypothesized that the C-terminal *AtNAA60*_{202–270} is responsible for the membrane association in plants. Transient expression of the C-terminally truncated *AtNAA60*_{1–205} protein fragment in fusion with GFP (GFP-*AtNAA60*_{1–205}) resulted in nucleocytoplasmic localization of GFP-*AtNAA60*_{1–205} in *Arabidopsis* leaf protoplasts and tobacco pavement cells (Figs 4b–e, S8a–e). Transiently expressed CFP-*AtNAA60*_{1–270} (named in Fig. 1 CFP-At5g16800) was localized at the plasma membrane in both plant species (Figs 1b–g, S2), implying that the C-terminal domain *AtNAA60*_{206–270} is necessary and sufficient for plasma membrane association. Indeed, when we fused this domain to the C-terminus of CFP (CFP-*AtNAA60*_{206–270}), the resulting fusion protein is associated with the plasma membrane (Figs 4f–i, S8f). Co-staining of the Golgi apparatus with SYP32 revealed a potential overlap with CFP-*AtNAA60*_{206–270} signal in *Arabidopsis* protoplasts (Fig. S8g–j), which has not been found with CFP-*AtNAA60*_{1–270}. These results suggest that the C-terminal domain of *AtNAA60* is sufficient for localization of the full-length *AtNAA60* at the plasma membrane.

Contribution of the *AtNAA60* C-terminus to membrane binding

The *in planta* deletion analysis of *AtNAA60* fused to fluorescent proteins demonstrate that the C-terminal domain, *AtNAA60*_{206–270}, is necessary and sufficient for localization of *AtNAA60* to the membrane. The predicted α -helix (P206–V230, $\alpha 5$) is amphipathic with a strong hydrophobic moment and the residues R218 and K227 positioned at the border of the hydrophobic/hydrophilic interface are able to snorkel into the membrane (Fig. 4j). These features classify $\alpha 5$ of *AtNAA60* as a canonical type A amphipathic helix (Segrest *et al.*, 1990).

Next, we tested the conformation of *AtNAA60*_{205–270} in the presence of liposomes and its interaction with liposomes mimicking plant plasma membrane lipid composition (Yoshida & Uemura, 1986; Uemura *et al.*, 1995; Grison *et al.*, 2015). Circular dichroism experiments revealed that *AtNAA60*_{205–270} is unstructured in solution and adopts a helical secondary structure only in the presence of liposomes. Trifluoroethanol (TFE), used to probe α -helix propensity (Stjepanovic *et al.*, 2011), also induces $\alpha 5$ helix formation (Fig. 4k). The intrinsic tryptophan fluorescence of *AtNAA60*_{205–270}, containing only the W239, presents a blue shift upon addition of liposomes, indicating interaction of the *AtNAA60* C-terminus with the liposomes (Fig. 4l). To confirm the binding of *AtNAA60*_{205–270} to the liposomes, we performed density gradient flotation assays. *AtNAA60*_{205–270} only floats when incubated with liposomes, whereas *AtNAA60*_{20–200} is always found in the bottom fraction (Fig. 4m). Therefore, we conclude that *AtNAA60*_{205–270} is necessary and sufficient for binding to plant plasma membrane-like liposomes.

Identification of *AtNAA60* substrates *in vivo*

The identification of *AtNAA60* as the first plasma membrane-resident N-terminal acetyltransferase prompted us to investigate its biological function *in vivo*. We therefore identified two homozygous T-DNA insertion mutants. The integration of the T-DNA in the first intron of At5g16800 caused significant destabilization of the *AtNAA60* transcript in *naa60-1* (Fig. 5a,b). In *naa60-2*, the T-DNA is inserted in the last exon of *AtNAA60* (Fig. S9a). The vegetative and generative growth of both mutants was indistinguishable from the wild type when grown under nonstressed conditions (Figs 5c,d, S9b). Because NAA60 is Golgi-localized and required for ribbon formation of Golgi stacks at the nucleus

Fig. 5 *In vivo* identification of *AtNAA60* substrates. (a) Schematic depiction of the *AtNAA60* gene. Black arrows represent exons and lines represent introns. The triangle indicates the T-DNA insertion site. Binding sites of the qRT-PCR primers are shown as gray arrows. Bar, 200 bp. (b) Quantification of relative *NAA60* transcript levels in leaves of 6-wk-old soil-grown *Arabidopsis* plants. Data represent mean \pm SE. Asterisks indicate significant differences between wild type and *naa60-1* (Student's *t*-test, $P < 0.001$, $n = 3$). (c) Top view on 7-wk-old wild type and *naa60-1 Arabidopsis thaliana* plants grown under short-day conditions. Bar, 2 cm. (d) Representative growth phenotype of 11-wk-old plants grown under short-day conditions. Bar, 2 cm. (e, f) Representative electron microscope images of the Golgi apparatus in roots of 1-wk-old wild type (e) and *naa60-1* (f) *Arabidopsis* seedlings. Bar, 100 nm. (g) N-terminal acetylation frequency of soluble proteins isolated from leaves of 6-wk-old *Arabidopsis* plants ($n = 3$ –4 from two or three individual pools of leaf tissue for each genotype). (h) Enzymatic activity of purified HisMBP-*AtNAA60* on diverse substrate peptides as determined by the transfer of isotope-labeled acetyl-group from acetyl-CoA. MQGR and MAPR are N-termini from *HsNAA60* substrates identified in Aksnes *et al.* (2015b). MQPT is the N-terminal sequence of DUF662 (At5g03660). Data represent mean \pm SE. Different letters indicate individual groups identified by pairwise comparisons with a Holm–Sidak, one-way ANOVA ($P < 0.05$, $n = 4$).

in humans, we determined Golgi-stack formation in the Arabidopsis wild type and the *naa60-1* mutant by electron microscopy. In contrast to the function of NAA60 in human cells, absence of *AtNAA60* in plant cells had no impact on the formation of the Golgi apparatus (Fig. 5e,f), which agrees with the exclusive localization of the full-length *AtNAA60* at the plasma membrane (Fig. 1b–g).

Next, we profiled the N-terminal acetylome in leaf cells of *naa60-1* to identify *AtNAA60* substrates *in vivo*. Characterization of more than 2059 N-terminal peptides from 1623 distinct nonredundant proteins by MS/MS analysis suggested that loss of *AtNAA60* function had no significant impact on the NTA at the global scale (Fig. 5g; Tables S5–S7). In total, 47% of the characterized N-termini in the leaves of wild type Arabidopsis are modified by NTA (Fig. 5g). Among them, 956 N-termini corresponded to peptides displaying the first Met (iMet) or the second amino acid unmasked by the removal of iMet by cytosolic MetAPs (Frottin *et al.*, 2009). In total, 51% of these experimentally identified acetylated N-termini in Arabidopsis were acetylated after removal of the iMet. The remainder are acetylated at the iMet (27%). Only one protein, At5g03660, was significantly less acetylated in *naa60-1*, suggesting that the plasma membrane localization of *AtNAA60* restricts the access of potential substrates to *AtNAA60* (Fig. 5g). Indeed, At5g03660 is a plasma membrane-localized protein that is enriched in purified plasmodesmata (Benschop *et al.*, 2007; Fernandez-Calvino *et al.*, 2011). *AtNAA60* acetylates a peptide representing the At5g03660 N-terminus (MQPTE) with the same efficiency as a human NAA60 substrate (MQGRR) (Figs 5h, S4d). By contrast, *AtNAA60* does not acetylate a peptide less efficiently, where a P is inserted in the second position of At5g03660 (MPQPT, Figs 5h, S4d), as suggested from the inhibitory role of P2 for substrate recognition by catalytic subunits of Nat complexes (Goetze *et al.*, 2009). Based on the membrane localization of both proteins, the decreased NTA frequency of At5g03660 in *naa60-1* and the acetylation of the At5g03660 N-terminus by *AtNAA60 in vitro*, we concluded that At5g03660 is a *bona fide AtNAA60* substrate.

Impact of NAA60 in plants upon protein-harming stress

Imprinting of the proteome by protein modifications contributes to the tolerance of plants towards protein harming stresses such as high sodium chloride (NaCl) concentration (Isayenkov & Maathuis, 2019). To understand the biological relevance of protein acetylation by the membrane-associated NAA60 under abiotic stress, we challenged *naa60-1* and the wild type with cytotoxic concentrations of NaCl during germination. Application of 120 mM NaCl decreased germination efficiency of *naa60-1* to 30% of control conditions, while germination efficiency of the wild type was not affected by this treatment (Fig. 6a,b). Also, *naa60-2* was more sensitive to high salt application when compared to the wild type (Fig. S9c,d). Transcriptional induction of the high salt responsive gene, *DREB2A*, verified the impact of the treatment applied here on the wild type (Fig. S10a). However, the high salt treatment had no significant impact on *AtNAA60* transcription (Fig. S10b). The decrease of

naa60-1 germination efficiency correlated with the applied NaCl concentration (Fig. S10c). Complementation of *naa60-1* with *AtNAA60-YFP* under control of the CaMV35S-pro results in wild-type-like tolerance towards high salt stress (Fig. 6a,b). The exclusive localization of *AtNAA60-YFP* at the plasma membrane of *naa60-1/CaMV35S_{pro}:AtNAA60-YFP* demonstrates the crucial function of NAA60 in this compartment under high salinity (Fig. S10d–f).

Discussion

Despite the prevalence of NTA in the plant proteome, the acetylation machinery has barely been characterized in plants. Thus far, only candidates for NatA, NatB and NatC have been experimentally confirmed in Arabidopsis (Pesaresi *et al.*, 2003; Linster *et al.*, 2015; Huber *et al.*, 2020).

In this study, we unambiguously identify a novel plasma membrane-localized NAA60-type N^α-acetyltransferase in the reference plant *A. thaliana*. We show that plant NAA60 acts post-translationally on a plasma membrane protein and contributes to high salt stress tolerance. *AtNAA60* crystal structures reveal the NAA60 substrate binding mode and elucidate its broad substrate specificity. We show that full-length *AtNAA60* is exclusively located at the plasma membrane and that its C-terminal region (residues 206–270) is necessary for plasma membrane binding *in vivo*. Sequence analysis of the *AtNAA60* C-terminus revealed a putative type A amphipathic α -helix (residues 206–230) with an explicit hydrophilic and hydrophobic face, suggesting a peripheral orientation towards the membranes. Indeed, the *AtNAA60* C-terminus forms an α -helix that associates with liposomes, mimicking plant plasma membranes and is necessary for liposome binding. Similarly, the *HsNAA60* C-terminus is essential for localization to the Golgi and is composed of two amphipathic helices (Aksnes *et al.*, 2017). In humans, the C-terminus has been shown to prefer binding to membranes containing phosphatidylinositol (PI4P; Aksnes *et al.*, 2017), which is also present in low amounts in plant plasma membranes (Cacas *et al.*, 2016). When compared, the length and hydrophobic moment of the combined two human helices is similar to that of the single amphipathic helix in Arabidopsis, suggesting similar membrane binding in both organisms. In addition, it has been shown that the residues following the two helices affect membrane-binding capacity in human (Aksnes *et al.*, 2017). This indicates that the exclusive plasma membrane localization of *AtNAA60* cannot be simply explained by differences in the amphipathic helices, but is encoded in the entire C-terminus. Of note, the lipid composition of the plant plasma membrane varies significantly with different environmental exposures (Uemura *et al.*, 1995), suggesting that *AtNAA60* needs to tolerate a wide range of lipid compositions in order to maintain plasma membrane binding.

Regardless of its novel localization, *AtNAA60* presents a similar substrate specificity as its human homolog (Aksnes *et al.*, 2015b). Compared to *AtNatB*, which requires an acidic residue following the iMet (Huber *et al.*, 2020), *AtNAA60* specificity is broad, as it acetylates the initiator methionine with little restrictions for the following amino acids. As human NAA60 displays

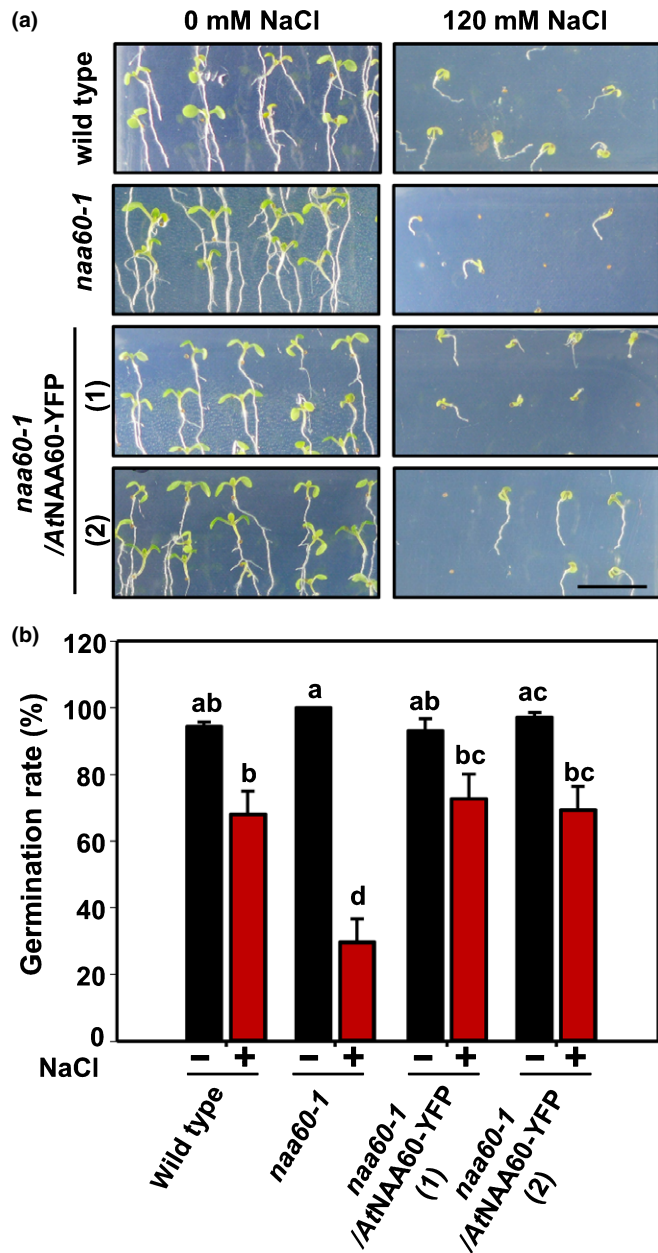


Fig. 6 *naa60-1* mutants are sensitive to NaCl stress. Seeds from wild type, *naa60-1* and two independent *naa60-1*/AtNAA60-YFP *Arabidopsis thaliana* lines were surface sterilized, stratified for 48 h, and germinated on 1× MS medium or 1× MS medium supplemented with 120 mM NaCl. Germination rate was quantified after 2 wk of growth under short-day conditions. (a) Representative sections of germinated and nongerminated seeds. Bar, 1 cm. (b) Quantification of the germination rate. Data represent mean ± SE. Different letters indicate individual groups identified by pairwise comparisons with a Holm–Sidak, one-way ANOVA ($P < 0.05$, $n = 3$ individual experiments with 24 seeds).

Kat activity *in vitro* (Chen *et al.*, 2016), we also tested the bifunctional Nat/Kat activity of the plant NAA60. We found that it preferentially acetylates protein N^α-termini, while the activity on internal N^ε-Lys-residues was marginal for the tested peptide. However, our results do not eliminate a potential side activity of plant NAA60 on internal Lys residues *in vivo*.

The structure of the enzymatic active part of AtNAA60 adopts the conserved GNAT-fold and has a similar overall structure to its human homolog (Chen *et al.*, 2016; Stove *et al.*, 2016). Furthermore, the structure of AtNAA60 with the new bisubstrate analog CoA-Ac-MVNAL allowed us to decipher the enzymatic mechanism and mode of substrate binding. The bisubstrate's first amino acid (M1_p) is involved in multiple contacts via its main chain and its sidechain is placed in a hydrophobic pocket. Ligand–protein contacts for the consecutive residues are not sidechain-specific. Moreover, the binding site for the second amino acid is solvent-exposed and there is no significant structure-based amino acid preference, apart from a tryptophan residue, which seems to be impossible due to steric clashes. This agrees with the GAP assays results (Fig. 2b), where no substrate with a tryptophan at the second position was found. The catalytic mechanism of AtNAA60 seems to be conserved with HsNAA50 and HsNAA60, as residues essential for activity are conserved. Moreover, a well-ordered water molecule, probably involved in base catalysis, is present in the active sites of HsNAA50 and HsNAA60 (Liszczak *et al.*, 2011; Stove *et al.*, 2016). The major structural differences between AtNAA60 and its human homolog are found in loop regions, with the loop β2–β3 in Arabidopsis being elongated, whereas the loop β3–β4 is of similar length but does not superimpose well. In both organisms, the loop β3–β4 is vital for protein stability as it folds back to the core of the enzyme (Stove *et al.*, 2016). However, in Arabidopsis back-folding is less pronounced, as it involves only the interaction of E97 and H154, whereas in human loop β3–β4 (residues E80, D81 and D83) interacts with the core enzyme (residues Y136, H138 and H159). Moreover, in contrast to HsNAA60, AtNAA60 is a monomer in the presence of AcCoA or CoA in solution. In the HsNAA60 dimer, the hairpin β6'–β7' blocks the peptide entry site of the second protomer, indicating that the observed dimer is an inactive form. Nevertheless, in both studies truncated protein versions were used for crystallization and oligomerization tests. Whether *in vivo* AtNAA60 or HsNAA60 dimerize at their respective membranes and whether the amphipathic helices play a role in oligomerization is not known. In agreement with the specific acetylation of membrane proteins by HsNAA60 (Aksnes *et al.*, 2015c), a global N-acetylome profiling approach revealed one plasmodesmata localized protein as substrate of NAA60 in plants. It can be concluded that the constraints for an NAA60 substrate are not sequence-based, but are the membrane localization of the substrates. The consequences of NTA for proteins localized at the membrane are currently unknown. However, NTA of cytosolic proteins affects protein stability in yeast, humans and Arabidopsis, suggesting that NTA is a significant determinant of protein fate in all eukaryotes (Hwang *et al.*, 2010; Shemorry *et al.*, 2013; Park *et al.*, 2015; Xu *et al.*, 2015). Remarkably, a large fraction of integral membrane proteins are also N-terminally acetylated in Holoarchaea, although the overall degree of NTA is only 14–19% in these prokaryotes (Falb *et al.*, 2006). This allows us to speculate on a conserved function of NTA for the fate of membrane proteins in prokaryotes and eukaryotes. In this respect, it is noteworthy that the Ac/N end rule pathway also degrades Cog1, a subunit of the Golgi-associated COG complex, and perilipin 2, a

lipid droplet-associated protein that is released upon nutrient stress (Shemorry *et al.*, 2013; Nguyen *et al.*, 2019). In plants, NTA also occurs post-translationally on nuclear-encoded plastid-localized proteins (Dinh *et al.*, 2015; Rowland *et al.*, 2015), and is suggested to affect stability of plastid proteins in the green alga *Chlamydomonas reinhardtii* (Bienvenut *et al.*, 2011).

The plasma membrane is the cellular interface that regulates the exchange of molecules and information between cells and their environment. Loss of the plasma membrane-resident NAA60 function in *naa60-1* does not affect plant growth and development under nonstressed conditions. By contrast, transient depletion of NAA60 induces defects in chromosomal segregation in *Drosophila melanogaster* cells (Van Damme *et al.*, 2011b), and inhibits cell proliferation in human cell lines (Yang *et al.*, 2011). The decreased cell proliferation in NAA60-depleted human cells is probably a direct consequence of Golgi ribbon fragmentation compromising mTOR (Aksnes *et al.*, 2015a; Gosavi *et al.*, 2018), which is the central regulator of cell proliferation in eukaryotes (Laplante & Sabatini, 2012; Dong *et al.*, 2017). Remarkably, expression of *DmNAA60* in NAA60-depleted human cells rescues the diminished cell proliferation phenotype, suggesting a conservation of the NAA60 function in animals (Yang *et al.*, 2011). The different physiological function of NAA60 in animals and plants appears to be predominantly caused by the organism-specific subcellular localization of NAA60, as *AtNAA60* and *HsNAA60* share broad and overlapping substrate specificities. Because perception of environmental cues and transport of ions and metabolites are vital functions of the plasma membrane and are executed by dynamically regulated plasma membrane-resident proteins (Wang *et al.*, 2018), we challenged *naa60-1* with surplus NaCl. The sensitivity of *naa60-1* and *naa60-2* towards enhanced salinity provides evidence for a relevant function of NTA on membrane proteins during stress. These results are in agreement with the critical role of the plasma membrane in osmoregulation of the cell (Schulz, 2011), and support the previously hypothesized role of NTA in plant stress responses (Linster & Wirtz, 2018). In the pathogen response, NTA tuned plant immunity by modulating the protein stability of an immune receptor via N-degron formation (Xu *et al.*, 2015). Salinity impairs plant growth via water stress, via excessive ion uptake and by oxidative stress due to the generation of reactive oxygen species (Isayenkov & Maathuis, 2019). If oxidized proteins accumulate, they tend to aggregate and become cytotoxic (Cohen *et al.*, 2006). Thus, destruction of misfolded proteins is critical for successful adaptation to high salt conditions. However, it is currently unclear how NAA60 contributes to salinity resistance due to the manifold impact of NTA on protein fate.

Conclusion

N-terminal protein acetylation is one of the most abundant protein modifications in humans and plants. In contrast to phosphorylation, which is catalyzed by thousands of specific kinases in humans and plants, only eight N-acetyltransferases are considered to imprint the proteomes of humans and Arabidopsis with acetylation marks. Here we uncover a novel plasma membrane-

resident N-acetyltransferase in Arabidopsis and identify a plasmodesmata-localized protein as its substrate. These findings demonstrate a remarkable evolution of the NTA machinery in the different phyla of eukaryotes: In humans and plants, membrane-associated N-acetyltransferases of the F-type acetylate post-translationally proteins in different membrane systems, while NTA is restricted to ribosomes in fungi. The C-terminal tail of NAA60 displays organism-specific adaptations and serves as the anchor for the selective membrane association in plants and humans. This organism-specific localization is an important trigger for the neofunctionalization of NAA60 in plants. Furthermore, we have demonstrated the functional relevance of post-translational NTA by NAA60 in the high salt stress response of plants. Our results shed light on the evolution of the enzymatic machinery that imprints more than 70% of cytosolic proteins in such diverse organisms as the fruit fly, Arabidopsis and humans, and opens new avenues to study the stimulus-induced dynamic adaptation of the N-acetylome in eukaryotes.

Acknowledgements

Data collection was performed at ESRF Grenoble beamlines ID23 and ID30B. We acknowledge the data storage service SDS@hd supported by the Ministry of Science, Research and the Arts Baden-Württemberg (MWK) and the German Research Foundation (DFG) through grant INST 35/1314-1 FUGG and INST 35/1503-1 FUGG. We thank C. Siegmann from the BZH/Cluster of Excellence:CellNetworks crystallization platform for protein crystallization, and G. Stier for initial cloning. We are grateful to M. Köhn, M. Fontanillo Dolz and N. Höfflin (Freiburg University) for support in the bisubstrate synthesis. We thank M. Mayer for access to the circular dichroism spectrophotometer and T. Söllner (Heidelberg University) for providing lipids. Electron microscopy was performed at the EM Core Facility of Heidelberg University and we are thankful to Steffi Gold for helping with sample preparation and Stefan Hillmer for microscopic analysis. The CG team benefitted from the support of the Labex Saclay Plant Sciences-SPS (ANR-10-LABX-0040-SPS) and used the facilities and expertise of the I2BC proteomic platform SICaPS, supported by IBiSA, Ile de France Region, Plan Cancer, CNRS and Paris-Sud University. We thank G. Bernal for the preparation of samples for GAP analysis. Research at Heidelberg was funded by the German Research Council (DFG) via Project-ID 201348542 - SFB 1036 (TP22 to IS and TP13 to MW) and the Leibniz programme (SI 586/6-1, to IS), and the ERA-CAPS Research Programme 'KatNat' (ANR-17-CAPS-0001-01 to IF, CG, MW). Research in CG's lab was supported by the French Agence Nationale de la Recherche agency (ANR-13-BSV6-0004). RH and IS are investigators of the Cluster of Excellence: CellNetworks. The authors declare no competing interests.

Author contributions

EL designed and performed the subcellular localization of NAA60, complementation of *naa60-1*, radioactive acetylation assay and quantification of the *naa60-1* germination efficiency,

and wrote the manuscript. DL designed and performed biochemical and structural experiments, analyzed data, collected and processed all X-ray diffraction data, designed and synthesized bisubstrate analog, and wrote the manuscript. TVD performed phenotypic characterization of the *naa60-1* mutants under control and stressed conditions, localized full-length NAA60 and quantified the radioactive acetylation assay. FAW performed cloning and helped with the initial crystallization screening and data collection. WL analyzed the subcellular localization of NAA60 truncations. AB performed HPLC-based enzyme activity measurements. MH analyzed the impact of NaCl on the *naa60-1* germination efficiency. PM performed and analyzed the qRT-PCR analysis. JK performed crystallization screening, processed all X-ray diffraction data sets, analyzed data and wrote the manuscript. KL designed and analyzed experiments, and wrote the manuscript. JS synthesized peptides for HPLC-based enzyme activity measurements. DS designed peptides for HPLC-based enzyme activity measurements. IF supervised and analyzed the HPLC-based enzyme activity experiments. CG, TM and WV conceived the N-terminomics analysis of WT, *Δ*NAA60 mutant and GAP assay, supervised the experiments and analyzed the data. RH, IS and MW designed and analyzed experiments, acquired funding, and wrote the manuscript. EL and DL contributed equally to this work.

ORCID

Willy V. Bienvenu  <https://orcid.org/0000-0003-4192-3920>
Annika Brünje  <https://orcid.org/0000-0002-8979-4606>
Iris Finkemeier  <https://orcid.org/0000-0002-8972-4026>
Carmela Giglione  <https://orcid.org/0000-0002-7475-1558>
Ruediger Hell  <https://orcid.org/0000-0002-6238-4818>
Jürgen Kopp  <https://orcid.org/0000-0001-5633-7399>
Karine Lapouge  <https://orcid.org/0000-0003-0620-9553>
Dominik Layer  <https://orcid.org/0000-0002-1577-7651>
Wiebke Leemhuis  <https://orcid.org/0000-0001-8729-5822>
Eric Linster  <https://orcid.org/0000-0001-7963-1400>
Thierry Meinnel  <https://orcid.org/0000-0001-5642-8637>
Pavlina Miklankova  <https://orcid.org/0000-0002-1170-5490>
Dirk Schwarzer  <https://orcid.org/0000-0002-7477-3319>
Julia Sindlinger  <https://orcid.org/0000-0002-7265-8093>
Irmgard Sinning  <https://orcid.org/0000-0001-9127-4477>
Markus Wirtz  <https://orcid.org/0000-0001-7790-4022>

References

- Aksnes H, Drazic A, Marie M, Arnesen T. 2016. First things first: vital protein marks by N-terminal acetyltransferases. *Trends in Biochemical Sciences* 41: 746–760.
- Aksnes H, Goris M, Stromland O, Drazic A, Waheed Q, Reuter N, Arnesen T. 2017. Molecular determinants of the N-terminal acetyltransferase Naa60 anchoring to the Golgi membrane. *Journal of Biological Chemistry* 292: 6821–6837.
- Aksnes H, Hole K, Arnesen T. 2015. Molecular, cellular, and physiological significance of N-terminal acetylation. *International Review of Cell and Molecular Biology* 316: 267–305.
- Aksnes H, Marie M, Arnesen T. 2015a. Holding it together: Naa60 at the Golgi. *Oncotarget* 6: 15726–15727.
- Aksnes H, Ree R, Arnesen T. 2019. Co-translational, post-translational, and non-catalytic roles of N-terminal acetyltransferases. *Molecular Cell* 73: 1097–1114.
- Aksnes H, Van Damme P, Goris M, Starheim KK, Marie M, Stove SI, Hoel C, Kalvik TV, Hole K, Glomnes N *et al.* 2015b. An organellar N^ε-acetyltransferase, *naa60*, acetylates cytosolic N termini of transmembrane proteins and maintains Golgi integrity. *Cell Reports* 10: 1362–1374.
- Armbruster L, Linster E, Boyer J-B, Brünje A, Eirich J, Stephan I, Bienvenu WV, Weidenhausen J, Meinnel T, Hell R *et al.* 2020. NAA50 is an enzymatically active N^ε-acetyltransferase that is crucial for the development and regulation of stress responses. *Plant Physiology*. doi: 10.1104/pp.20.00222.
- Arnesen T. 2011. Towards a functional understanding of protein N-terminal acetylation. *PLoS Biology* 9: e1001074.
- Arnesen T, Van Damme P, Polevoda B, Helsen K, Evjenth R, Colaert N, Varhaug JE, Vandekerckhove J, Lillehaug JR, Sherman F *et al.* 2009. Proteomics analyses reveal the evolutionary conservation and divergence of N-terminal acetyltransferases from yeast and humans. *Proceedings of the National Academy of Sciences, USA* 106: 8157–8162.
- Benschop JJ, Mohammed S, O'Flaherty M, Heck AJR, Slijper M, Menke FLH. 2007. Quantitative phosphoproteomics of early elicitor signaling in *Arabidopsis*. *Molecular & Cellular Proteomics* 6: 1198–1214.
- Bienvenu WV, Brünje A, Boyer J-B, Mühlenbeck JS, Bernal G, Lassowskat I, Dian C, Linster E, Dinh TV, Koskela MM *et al.* 2020. Dual lysine and N-terminal acetyltransferases reveal the complexity underpinning protein acetylation. *Molecular Systems Biology*. doi: 10.15252/msb.20209464.
- Bienvenu WV, Espagne C, Martinez A, Majeran W, Valot B, Zivy M, Vallon O, Adam Z, Meinnel T, Giglione C. 2011. Dynamics of post-translational modifications and protein stability in the stroma of *Chlamydomonas reinhardtii* chloroplasts. *Proteomics* 11: 1734–1750.
- Bienvenu WV, Giglione C, Meinnel T. 2017. SILProNAQ: a convenient approach for proteome-wide analysis of protein N-termini and N-terminal acetylation quantitation. *Methods in Molecular Biology* 1574: 17–34.
- Buchan DWA, Jones DT. 2019. The PSIPRED protein analysis workbench: 20 years on. *Nucleic Acids Research* 47: W402–W407.
- Cacas J-L, Buré C, Grosjean K, Gerbeau-Pissot P, Lherminier J, Rombouts Y, Maes E, Bossard C, Gronnier J, Furt F *et al.* 2016. Revisiting plant plasma membrane lipids in tobacco: a focus on sphingolipids. *Plant Physiology* 170: 367–384.
- Chen JY, Liu L, Cao CL, Li MJ, Tan K, Yang X, Yun CH. 2016. Structure and function of human Naa60 (NatF), a Golgi-localized bi-functional acetyltransferase. *Scientific Reports* 6: 31425.
- Clough SJ, Bent AF. 1998. Floral dip: a simplified method for *Agrobacterium*-mediated transformation of *Arabidopsis thaliana*. *The Plant Journal* 16: 735–743.
- Cohen E, Bieschke J, Perciavalle RM, Kelly JW, Dillin A. 2006. Opposing activities protect against age-onset proteotoxicity. *Science* 313: 1604–1610.
- Deng S, Magin RS, Wei X, Pan B, Petersson EJ, Marmorstein R. 2019. Structure and mechanism of acetylation by the N-terminal dual enzyme NatA/Naa50 complex. *Structure* 27: 1057–1070.
- Dinh TV, Bienvenu WV, Linster E, Feldman-Salit A, Jung VA, Meinnel T, Hell R, Giglione C, Wirtz M. 2015. Molecular identification and functional characterization of the first N^ε-acetyltransferase in plastids by global acetylome profiling. *Proteomics* 15: 2426–2435.
- Dong Y, Silbermann M, Speiser A, Forieri I, Linster E, Poschet G, Allboje Samami A, Wanatabe M, Sticht C, Teleman AA *et al.* 2017. Sulfur availability regulates plant growth via glucose-TOR signaling. *Nature Communications* 8: 1174.
- Drazic A, Aksnes H, Marie M, Boczkowska M, Varland S, Timmerman E, Foy H, Glomnes N, Rebowski G, Impens F *et al.* 2018. NAA80 is actin's N-terminal acetyltransferase and regulates cytoskeleton assembly and cell motility. *Proceedings of the National Academy of Sciences, USA* 115: 4399–4404.
- Drazic A, Myklebust LM, Ree R, Arnesen T. 2016. The world of protein acetylation. *Biochimica et Biophysica Acta* 1864: 1372–1401.

- Falb M, Aivaliotis M, Garcia-Rizo C, Bisle B, Tebbe A, Klein C, Konstantinidis K, Siedler F, Pfeiffer F, Oesterheld D. 2006. Archaeal N-terminal protein maturation commonly involves N-terminal acetylation: a large-scale proteomics survey. *Journal of Molecular Biology* 362: 915–924.
- Fernandez-Calvino L, Faulkner C, Walshaw J, Saalbach G, Bayer E, Benitez-Alfonso Y, Maule A. 2011. Arabidopsis plasmodesmal proteome. *PLoS ONE* 6: e18880.
- Frottin F, Espagne C, Traverso JA, Mauve C, Valot B, Lelarge-Trouverie C, Zivy M, Noctor G, Meinel T, Giglione C. 2009. Cotranslational proteolysis dominates glutathione homeostasis to support proper growth and development. *Plant Cell* 21: 3296–3314.
- Gautschi M, Just S, Mun A, Ross S, Rucknagel P, Dubaquié Y, Ehrenhofer-Murray A, Rospert S. 2003. The yeast N²-acetyltransferase NatA is quantitatively anchored to the ribosome and interacts with nascent polypeptides. *Molecular and Cellular Biology* 23: 7403–7414.
- Geldner N, Denervaud-Tendon V, Hyman DL, Mayer U, Stierhof YD, Chory J. 2009. Rapid, combinatorial analysis of membrane compartments in intact plants with a multicolor marker set. *The Plant Journal* 59: 169–178.
- Gibbs DJ. 2015. Emerging functions for N-terminal protein acetylation in plants. *Trends in Plant Science* 20: 599–601.
- Goetze S, Qeli E, Mosimann C, Staes A, Gerrits B, Roschitzki B, Mohanty S, Niederer EM, Laczko E, Timmerman E *et al.* 2009. Identification and functional characterization of N-terminally acetylated proteins in *Drosophila melanogaster*. *PLoS Biology* 7: e1000236.
- Gookin TE, Assmann SM. 2014. Significant reduction of BiFC non-specific assembly facilitates in planta assessment of heterotrimeric G-protein interactors. *The Plant Journal* 80: 553–567.
- Gosavi P, Houghton FJ, McMillan PJ, Hanssen E, Gleeson PA. 2018. The Golgi ribbon in mammalian cells negatively regulates autophagy by modulating mTOR activity. *Journal of Cell Science* 131: jcs211987.
- Gottlieb L, Marmorstein R. 2018. Structure of human NatA and its regulation by the huntingtin interacting protein HYPK. *Structure* 26: 925–935.e8.
- Grisson MS, Brocard L, Fouillen L, Nicolas W, Wewer V, Dörmann P, Nacir H, Benitez-Alfonso Y, Claverol S, Germain V *et al.* 2015. Specific membrane lipid composition is important for plasmodesmata function in Arabidopsis. *Plant Cell* 27: 1228–1250.
- Hong H, Cai Y, Zhang S, Ding H, Wang H, Han A. 2017. Molecular basis of substrate specific acetylation by N-terminal acetyltransferase NatB. *Structure* 25: 641–649.e3.
- Huber M, Bienvenu WV, Linster E, Stephan I, Armbruster L, Sticht C, Layer DC, Lapouge K, Meinel T, Sinning I *et al.* 2020. NatB-mediated N-terminal acetylation affects growth and abiotic stress responses. *Plant Physiology* 182: 792–806.
- Foy H, Jones JE, Lewallen D, Narawane R, Varhaug JE, Thompson PR, Arnesen T. 2013. Design, synthesis, and kinetic characterization of protein N-terminal acetyltransferase inhibitors. *ACS Chemical Biology* 8: 1121–1127.
- Hwang CS, Shemorry A, Varshavsky A. 2010. N-terminal acetylation of cellular proteins creates specific degradation signals. *Science* 327: 973–977.
- Isayenkov SV, Maathuis FJM. 2019. Plant salinity stress: many unanswered questions remain. *Frontiers in Plant Science* 10: 80–91.
- Koskela MM, Brunje A, Ivanauskaite A, Grabsztunowicz M, Lassowskat I, Neumann U, Dinh TV, Sindlinger J, Schwarzer D, Wirtz M *et al.* 2018. Chloroplast acetyltransferase NSI is required for state transitions in *Arabidopsis thaliana*. *Plant Cell* 30: 1695–1709.
- Laplante M, Sabatini DM. 2012. mTOR signaling in growth control and disease. *Cell* 149: 274–293.
- Linster E, Stephan I, Bienvenu WV, Maple-Groden J, Myklebust LM, Huber M, Reichelt M, Sticht C, Geir Moller S, Meinel T *et al.* 2015. Downregulation of N-terminal acetylation triggers ABA-mediated drought responses in Arabidopsis. *Nature Communications* 6: 7640.
- Linster E, Wirtz M. 2018. N-terminal acetylation: an essential protein modification emerges as an important regulator of stress responses. *Journal of Experimental Botany* 69: 4555–4568.
- Liszcak G, Arnesen T, Marmorstein R. 2011. Structure of a ternary Naa50p (NAT5/SAN) N-terminal acetyltransferase complex reveals the molecular basis for substrate-specific acetylation. *Journal of Biological Chemistry* 286: 37002–37010.
- Liszcak G, Goldberg JM, Foy H, Petersson EJ, Arnesen T, Marmorstein R. 2013. Molecular basis for N-terminal acetylation by the heterodimeric NatA complex. *Nature Structural & Molecular Biology* 20: 1098–1105.
- Nguyen KT, Lee CS, Mun SH, Truong NT, Park SK, Hwang CS. 2019. N-terminal acetylation and the N-end rule pathway control degradation of the lipid droplet protein PLIN2. *Journal of Biological Chemistry* 294: 379–388.
- Park SE, Kim JM, Seok OH, Cho H, Wadas B, Kim SY, Varshavsky A, Hwang CS. 2015. Control of mammalian G protein signaling by N-terminal acetylation and the N-end rule pathway. *Science* 347: 1249–1252.
- Pesaresi P, Gardner NA, Masiero S, Dietzmann A, Eichacker L, Wickner R, Salamini F, Leister D. 2003. Cytoplasmic N-terminal protein acetylation is required for efficient photosynthesis in Arabidopsis. *Plant Cell* 15: 1817–1832.
- Ponomarenko EA, Poverennaya EV, Ilgisonis EV, Pyatnitskiy MA, Kopylov AT, Zgoda VG, Lisitsa AV, Archakov AI. 2016. The size of the human proteome: the width and depth. *International Journal of Analytical Chemistry* 2016: 1–6.
- Rathore OS, Faustino A, Prudencio P, Van Damme P, Cox CJ, Martinho RG. 2016. Absence of N-terminal acetyltransferase diversification during evolution of eukaryotic organisms. *Scientific Reports* 6: 21304.
- Rowland E, Kim J, Bhuiyan NH, van Wijk KJ. 2015. The Arabidopsis chloroplast stromal N-terminome: complexities of amino-terminal protein maturation and stability. *Plant Physiology* 169: 1881–1896.
- Schulz B. 2011. Functional classification of plant plasma membrane transporters. In: Murphy AS, Schulz B, Peer W, eds. *The plant plasma membrane*. Berlin: Springer, 131–176.
- Segrest JP, De Loof H, Dohlman JG, Brouillette CG, Anantharamaiah G. 1990. Amphipathic helix motif: classes and properties. *Proteins: Structure, Function, and Bioinformatics* 8: 103–117.
- Shemorry A, Hwang CS, Varshavsky A. 2013. Control of protein quality and stoichiometries by N-terminal acetylation and the N-end rule pathway. *Molecular Cell* 50: 540–551.
- Skaff DA, Mizioroko HM. 2010. A visible wavelength spectrophotometric assay suitable for high-throughput screening of 3-hydroxy-3-methylglutaryl-CoA synthase. *Analytical Biochemistry* 396: 96–102.
- Sparkes IA, Runions J, Kearns A, Hawes C. 2006. Rapid, transient expression of fluorescent fusion proteins in tobacco plants and generation of stably transformed plants. *Nature Protocols* 1: 2019–2025.
- Starheim KK, Arnesen T, Rynningen A, Varhaug JE, Lillehaug JR. 2008. Identification of the human N(alpha)-acetyltransferase complex B (hNatB): a complex important for cell-cycle progression. *Biochemical Journal* 415: 325–331.
- Stjepanovic G, Kapp K, Bange G, Graf C, Parlitz R, Wild K, Mayer MP, Sinning I. 2011. Lipids trigger a conformational switch that regulates signal recognition particle (SRP)-mediated protein targeting. *Journal of Biological Chemistry* 286: 23489–23497.
- Stove SI, Magin RS, Foy H, Haug BE, Marmorstein R, Arnesen T. 2016. Crystal structure of the golgi-associated human Nalpha-acetyltransferase 60 reveals the molecular determinants for substrate-specific acetylation. *Structure* 24: 1044–1056.
- Uemura M, Joseph RA, Steponkus PL. 1995. Cold acclimation of *Arabidopsis thaliana* (effect on plasma membrane lipid composition and freeze-induced lesions). *Plant Physiology* 109: 15–30.
- Van Damme P, Evjenth R, Foy H, Demeyer K, De Bock PJ, Lillehaug JR, Vandekerckhove J, Arnesen T, Gevaert K. 2011a. Proteome-derived peptide libraries allow detailed analysis of the substrate specificities of N²-acetyltransferases and point to hNaa10p as the post-translational actin N²-acetyltransferase. *Molecular & Cellular Proteomics* 10: 004580.
- Van Damme P, Hole K, Pimenta-Marques A, Helsens K, Vandekerckhove J, Martinho RG, Gevaert K, Arnesen T. 2011b. NatF contributes to an evolutionary shift in protein N-terminal acetylation and is important for normal chromosome segregation. *PLoS Genetics* 7: e1002169.
- Vetting MW, S de Carvalho LP, Yu M, Hegde SS, Magnet S, Roderick SL, Blanchard JS. 2005. Structure and functions of the GNAT superfamily of acetyltransferases. *Archives of Biochemistry and Biophysics* 433: 212–226.
- Wang L, Xue Y, Xing J, Song K, Lin J. 2018. Exploring the spatiotemporal organization of membrane proteins in living plant cells. *Annual Review of Plant Biology* 69: 525–551.

- Weyer FA, Gumiero A, Lapouge K, Bange G, Kopp J, Sinning I. 2017. Structural basis of HypK regulating N-terminal acetylation by the NatA complex. *Nature Communications* 8: 15726.
- Xu F, Huang Y, Li L, Gannon P, Linster E, Huber M, Kapos P, Bienvenut W, Polevoda B, Meinnel T *et al.* 2015. Two N-terminal acetyltransferases antagonistically regulate the stability of a nod-like receptor in *Arabidopsis*. *Plant Cell* 27: 1547–1562.
- Yang X, Yu W, Shi L, Sun L, Liang J, Yi X, Li Q, Zhang Y, Yang F, Han X *et al.* 2011. HAT4, a Golgi apparatus-anchored B-type histone acetyltransferase, acetylates free histone H4 and facilitates chromatin assembly. *Molecular Cell* 44: 39–50.
- Yoo SD, Cho YH, Sheen J. 2007. *Arabidopsis* mesophyll protoplasts: a versatile cell system for transient gene expression analysis. *Nature Protocols* 2: 1565–1572.
- Yoshida S, Uemura M. 1986. Lipid composition of plasma membranes and tonoplasts isolated from etiolated seedlings of mung bean (*Vigna radiata*, L.). *Plant Physiology* 82: 807–812.

Supporting Information

Additional Supporting Information may be found online in the Supporting Information section at the end of the article.

Fig. S1 Structure-based sequence alignment and *NAA60* transcript levels.

Fig. S2 Subcellular localization of full-length *AtNAA60* in *A. thaliana* protoplasts.

Fig. S3 Protein sequence alignment of putative plant NAA60.

Fig. S4 Analytical SEC, SEC-MALS and catalytic activity of *AtNaa60*₂₀₋₂₀₀.

Fig. S5 Structure of the CoA-Ac-MVNAL and crystal structures of *AtNAA60*.

Fig. S6 Interaction between *AtNAA60*₂₀₋₂₀₀ and CoA-Ac-MVNAL and stability of *AtNAA60* mutants.

Fig. S7 Superimpositions of *AtNAA60* and *HsNAA60* structures.

Fig. S8 Contribution of *AtNAA60* C-terminus to the subcellular localization.

Fig. S9 Characterization of *naa60-2*.

Fig. S10 Impact of NaCl on the germination of *naa60-1* seedlings.

Methods S1 Protein purification and crystallization.

Methods S2 Data collection and structure determination.

Methods S3 Determination of acetyltransferase activity with the microplate assay.

Methods S4 Determination of acetyltransferase activity with radioactively labeled AcCoA.

Methods S5 Peptide synthesis and comparison of Nat and Kat acetyltransferase assay.

Methods S6 Inhibition assays with CoA-Ac-MVNAL.

Methods S7 NanoDSF measurements.

Methods S8 Microscale thermophoresis measurements.

Methods S9 Preparation of plasma membrane-like liposomes.

Methods S10 Circular dichroism spectroscopy.

Methods S11 Intrinsic tryptophan fluorescence.

Methods S12 Density gradient flotation assays.

Methods S13 Electron microscopy

Table S1 List of primers.

Table S2 Results of the BLAST search with *HsNAA60* in the *Arabidopsis* proteome.

Table S3 List of N-terminal acetylated peptides retrieved from the GAP assay of *AtNAA60*.

Table S4 Crystallographic data and refinement statistics for *AtNaa60*.

Table S5 List of all identified N-termini.

Table S6 List of the identified nonredundant proteins.

Table S7 Processed data of the SILProNAQ approach.

Please note: Wiley Blackwell are not responsible for the content or functionality of any Supporting Information supplied by the authors. Any queries (other than missing material) should be directed to the *New Phytologist* Central Office.